Up-cycling of vitrified bottom ash from MSWI into glass-ceramic foams by means of ‘inorganic gel casting’ and sinter-crystallization

Construction and Building Materials 192 (2018) 133–140

Contents lists available at ScienceDirect

Construction and Building Materials

journal homepage: www.elsevier.com/locate/conbuildmat

Up-cycling of vitrified bottom ash from MSWI into glass-ceramic foams by means of 'inorganic gel casting' and sinter-crystallization

Acacio Rincon Romero [a], Milena Salvo [b], Enrico Bernardo [a,*]

[a] Department of Industrial Engineering, University of Padova, Italy
[b] Department of Applied Science and Technology, Politecnico di Torino, Turin, Italy

HIGHLIGHTS

- 'Inorganic gel casting' feasible for highly porous glass-ceramics from vitrified MSWI bottom ash.
- Hardening achieved with a low molarity alkaline solution, by formation of carbonate phases.
- Hardened foams transformed into glass-ceramics by low temperature sinter-crystallisation.
- Leaching of heavy metals from final product remaining under the thresholds specifications.

ARTICLE INFO

Article history:
Received 11 June 2018
Received in revised form 21 September 2018
Accepted 15 October 2018

Keywords:
Vitrification
MSWI bottom ash
Glass-ceramic foams
Alkali activation

ABSTRACT

The transformation of vitrified waste, such as bottom ash from municipal waste incineration, into cellular glass-ceramics is convenient, if the additional processing is simple and inexpensive. The present paper aims at presenting a possible route to achieve this goal, based on the recently proposed mechanical foaming of alkali-activated suspensions of waste glass powders, followed by sinter-crystallization at moderate temperatures (from 800 to 900 °C). Compared to previously studied glasses, in this experiment bottom ash-derived glass suspensions underwent progressive hardening at low alkali molarity and in limited times. The firing did not alter the open-celled structure that had developed upon low temperature foaming, owing to a significant crystallization. With an overall porosity of 80%, the optimized foams exhibited a remarkable compressive strength (>6 MPa). Finally, the process had no negative impact on the leaching of toxic elements, which remained well below the thresholds for inert materials.

1. Introduction

The total amount of municipal solid waste (MSW) generated in EU-28 by 2016 was 246 million tonnes, out of which up to 66 million tonnes were incinerated [1]. The main goals of incineration are the destruction of hazardous organic substances, the prevention of their dispersion in the environment, the reduction in volume of the initial waste, the reduction of the landfill space, and energy recovery. Bottom ash is one of the final residues from municipal solid waste incineration (MSWI); it represents about 10 vol% and approximately 20–30 wt% of the initial waste treated in the process [2,3].

Bottom ash presents a risk of heavy metal leaching, therefore suitable pre-treatments should be applied before it is landfilled or reused as a secondary raw material. However, its direct reuse is not feasible, and a delicate balance between stabilization costs and economic benefits from using bottom ash as an alternative raw material need to be studied carefully [4,5].

The building industry represents an excellent target for the valorisation of properly treated bottom ash. Depending on the formulations, bottom ash may be used in the form of aggregates, in the foundations of road constructions [6,7] and in concrete production, to replace natural aggregates [8], or as a reactive component, again in concretes, owing to its pozzolanic characteristics [9,10]. However, it should be observed that the presence of metallic aluminium or metallic zinc and chlorides leads to the long-term degradation of concrete, and the immobilisation of the heavy metals may not be complete [9,11].

Waste vitrification is one the most effective techniques available to achieve the complete stabilisation of heavy metals [12]. When applied to MSWI bottom ash, vitrification destroys dioxins and the other hazardous organic components that are present in them, determines a significant reduction in volume (60%) and yields a highly homogeneous glass that can be used in many

* Corresponding author. Fax: +39 049 8275505.
E-mail address: enrico.bernardo@unipd.it (E. Bernardo).

https://doi.org/10.1016/j.conbuildmat.2018.10.135
0950-0618/

applications [13]. Even if the high energy demand is a significant drawback of the process, the transformation of the by-products to a more valuable product can compensate for the cost and help avoiding the disposal fees [13].

Vitrified bottom ash can be used as another replacement of natural aggregates or as a pozzolanic additive in concrete [14–16], but the most interesting applications depend on its glassy nature. Waste-derived glass may be used as raw material for classical glass-based products, such as glass fibres [17], ceramic glazes [18] and, above all, glass-ceramic tiles [19–21].

Among the waste-derived glass-based materials, cellular glasses and glass-ceramics are particularly interesting because of their unique combination of low thermal conductivity, high mechanical strength and high chemical and thermal stability [13]. Compared to polymeric insulators, glass-based foams are non-flammable, although undoubtedly more expensive. The significant production costs are mostly due to the difficult control of the viscous flow sintering of the glass, with a concurrent gas evolution, owing to decomposition or oxidation reactions (Quiam et al., as an example, foamed vitrified bottom ash through the decomposition of a calcium carbonate additive [22]). The balance is even more delicate in the case of waste-derived glasses, which undergo crystallization upon sintering.

This investigation on cellular glass-ceramics from vitrified bottom ash was essentially conceived to assess the suitability of an alternative, recently established method, which is based on the alkali activation of the aqueous suspensions of glass powders [23,24] or glass-slag mixtures [25,26]. In this process, the suspensions undergo progressive hardening through the partial dissolution of glass and the formation of C-S-H (calcium-silicate-hydrated) compounds as the binding phase; before complete setting, the mixtures are foamed by intensive mechanical stirring, with the help of a surfactant. The thus obtained "green" foams are later subjected to viscous flow sintering, or sinter-crystallization, for glasses sensitive to surface nucleation. The viscous flow, besides joining adjacent glass particles, can reshape the pores obtained upon low temperature foaming [23]; however, in the case of significant crystallization, the increase in the viscosity of the softened glass caused by crystal inclusions 'freezes' the microstructural evolution, so that the open-celled structures substantially remain unaltered [24,26].

The specific glass here adopted led to a different hardening mechanism at a low temperature. Glass suspensions could be consolidated by means of an activating solution of particularly low molarity, compared to the ones used for geopolymers (also based on bottom ash) [27]. Owing to the substantial crystallization that was reached, the obtained glass-ceramic foams exhibited particularly remarkable specific strength values.

2. Experimental procedure

The starting material consisted of vitrified bottom ash (VBA) from a north Italian municipal solid waste incinerator (MSWI), which was melted at 1450 °C without adding any vitrifying agent. The vitrification process and the characteristics of the final vitrified bottom ash (VBA) are reported elsewhere [14]. The chemical composition of the obtained VBA is shown in Table 1.

The VBA was milled and sieved under 75 μm. The powders were suspended in an aqueous solution of 2.5 M NaOH (reagent grade, Sigma– Aldrich, Gillingham, UK), to a total solid loading of 70 wt%. The mixture was kept under mechanical stirring (500 rpm) at room temperature for 2 h, to achieve the partial dissolution of glass and a good dispersion of the remaining undissolved particles in the slurry.

A 4 wt% Triton X-100 solution (polyoxyethylene octyl phenyl ether – $C_{14}H_{22}O(C_2H_4O)n$, n = 9–10, Sigma-Aldrich, Gillingham, UK) was added to the glass suspension, which was then subjected to intensive mechanical stirring (2000 rpm, for 10 min). Some samples were also obtained after a pre-curing step of 1 h at 70 °C; this step was previously found to increase the pseudoplasticity of glass slurries by promoting gelification [23].

Table 1
Chemical composition (expressed in wt%) of the vitrified bottom ash.

Oxide (wt%)	Vitrified bottom ash (VBA)
SiO_2	51.7
Al_2O_3	10.9
CaO	16.2
Na_2O	6.9
Fe_2O_3	5.8
MgO	4.1
K_2O	1.6
TiO_2	0.7
BaO	0.2
ZnO	0.2
MnO	0.1
Others	Balance

The thus obtained wet foams were kept at 70 °C for 24 h in sealed polystyrene cylindrical moulds to complete the hardening. After demoulding, a thermal treatment was applied at 800–900 °C for 1 h in air (10 °C/min heating rate).

Selected samples were subjected to thermal analysis (TGA, Mettler Toledo TGA/DSC 3+, Zurich, Switzerland) operating at 10 °C/min in static air, from room temperature up to 800–900 °C. Fourier-transform infrared spectroscopy (FTIR, FTIR model 2000, Perkin Elmer Waltham, MA, USA) was performed, operating in absorbance mode, with a 4 cm^{-1} resolution for 32 scans in the 4500–400 cm^{-1} region.

The morphological and microstructural characterisations were executed by means of optical stereomicroscopy (AxioCam ERc 5s Microscope Camera, Carl Zeiss Microscopy, Thornwood, New York, US) and scanning electron microscopy (FEI Quanta 200 ESEM, Eindhoven, The Netherlands). The mineralogical analysis was conducted by means of X-ray diffraction (XRD) (Bruker D8 Advance, Karlsruhe, Germany), using CuKα radiation, 40 kV–40 mA, 2θ = 10–70°, a step size of 0.02° and a counting time of 0.5–2 s, with a position sensitive detector (LinxEye, Bruker AXS, Karlsruhe, Germany). The phase identification was completed using the Match!® programme package (Crystal Impact GbR, Bonn, Germany), supported by data from the PDF-2 database (ICDD-International Centre for Diffraction Data, Newtown Square, PA, USA).

The geometric density (ρ_g) of the fired foams was evaluated by considering the mass-to-volume ratio. The apparent (ρ_a) and the true density (ρ_t) were measured using a helium pycnometer (Micromeritics AccuPyc 1330, Norcross, GA), operating on bulk or finely crushed samples, respectively. The three density values (ρ_g, ρ_a, and ρ_t) were used to compute the amounts of open and closed porosity. Compression tests were conducted using an Instron 1121 UTS (Instron, Danvers, MA) machine, with a cross-head speed of 0.5 mm/min, employing foam samples of about 10 mm × 10 mm × 10 mm, which had been cut from larger specimens. Each data point corresponded to 9–10 samples.

The heavy metal release was evaluated according to the leaching procedure outlined in the European Standard for waste toxicity evaluation (EN 12457-2). Fragments below 4 mm were placed in distilled water, with a pH value of ≈7, for a liquid/solid ratio of 10, and were then softly stirred at 25 °C for 24 h. The solutions were filtered through a 0.6 μm filter and analysed using inductively coupled plasma (ICP; SPECTRO Analytical Instruments GmbH, Kleve, Germany).

3. Results and discussion

Fig. 1 reports the FTIR spectra of the VBA at the as received state, after hardening and after sintering. The two activated VBA plots correspond to the hardened state achieved with or without a pre-curing step (lasting 1 h); the two plots for the sintered VBA correspond to thermal treatments at 800 and 900 °C.

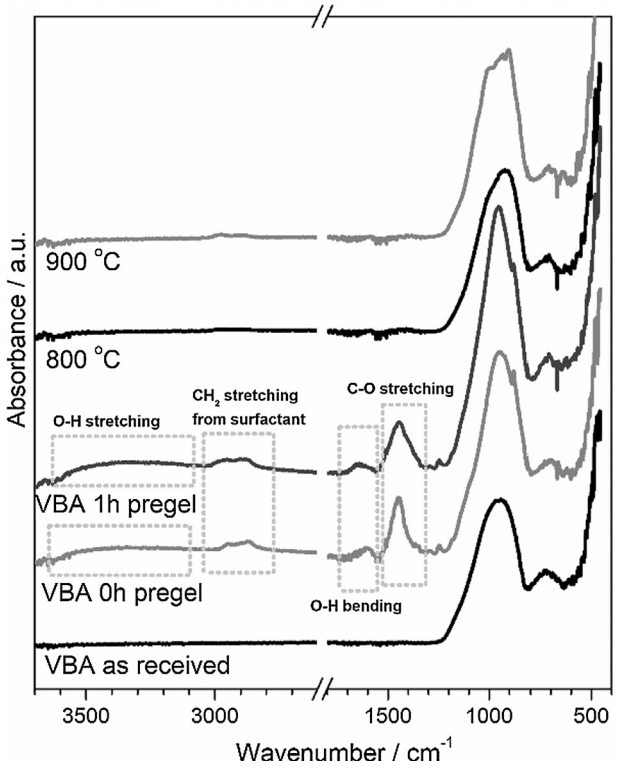

Fig. 1. FTIR analysis of VBA glass before and after foaming (with and without a pre-curing step at 70 °C for 1 h) and after heat treatments at 800 and 900 °C.

The FTIR spectrum of the original vitrified bottom ash presented a broad band between 950 and 1050 cm^{-1}, which was attributed to the asymmetric tension of the Si–O–Si and Al–O–Si groups. This band shifted to higher wavenumber values, and became narrower and more intense in the hardened foams: this effect could be associated with the polycondensation reactions that occur after alkali activation [28,29]. Sintering at 800 °C almost brought the VBA to the starting conditions, whereas the treatment at 900 °C led to the splitting of the band in several peaks, which may have been due to crystallization, i.e. more ordered structures.

Bands corresponding to the stretching modes (centred at about 3400 cm^{-1}) and to the bending vibration (at around 1638 cm^{-1}) of the OH groups were poorly visible in the hardened VBA. This suggests a limited formation of hydrated calcium silicate compounds (C–S–H), compared to previous experiments [23–25]. However, a quite strong band was noted at around 1458 cm^{-1}, which was attributed to the stretching vibration of C–O, but again only for the activated VBA. In addition, the sharp band at 875 cm^{-1} was attributed to the out-of-plane bending of CO_3^{2-}, thus suggesting that the hardening of the VBA was due also to carbonation. The formation of carbonates was also observed in previous studies [27,30]. Finally, the band at about 2800 cm^{-1}, but only for the activated VBA, could have been due to CH_2 stretch vibrations of the surfactant.

A confirmation of the findings of infrared spectroscopy was provided by high resolution X-ray diffraction analysis (with patterns collected with a position sensitive detector, yielding a distinctive high signal-to-noise ratio, operating with steps of 2θ = 0.02° and a counting time of 2 s), shown in Fig. 2. The activation, even with no pre-curing step, determined some modifications of the 'amorphous halo' of VBA glass; the limited intensity of the peaks did not allow for a precise phase identification, except for sodium hydrogen carbonate hydrate (trona, $Na_3H(CO_3)_2{\cdot}2H_2O$, PDF#29-1447). The

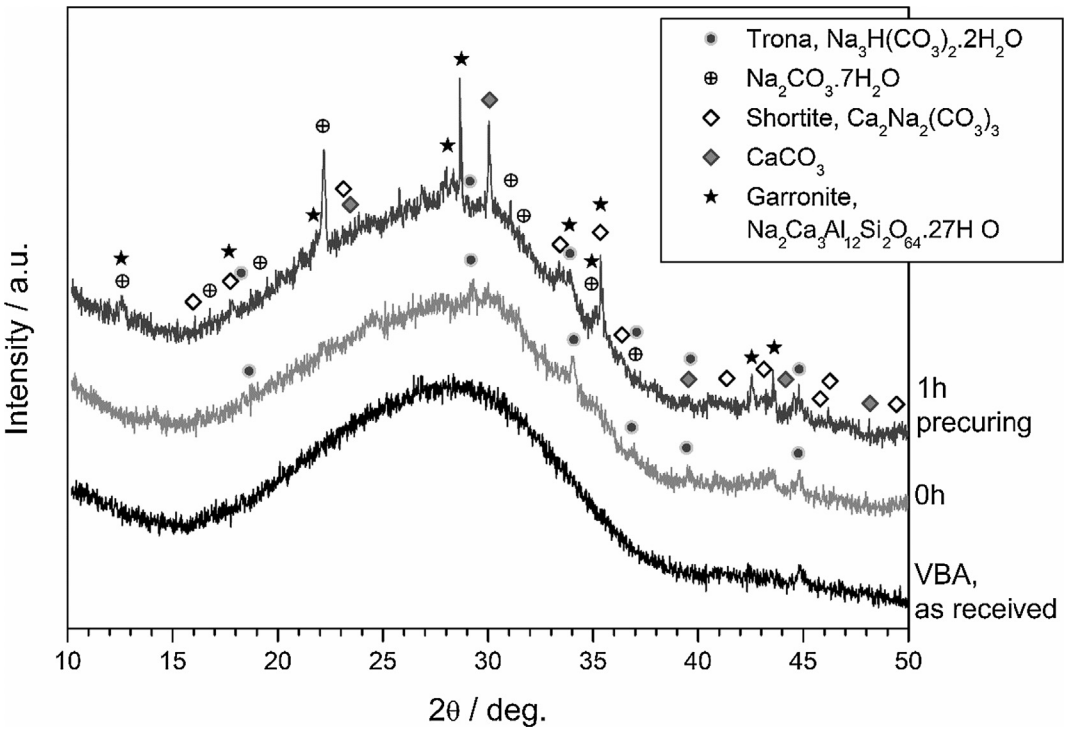

Fig. 2. Mineralogical analysis of VBA, in the as received conditions and after activation (precuring time of 0–1 h).

application of a pre-curing step (1 h) led to the development of quite well distinguishable phases, such as sodium carbonate hydrate ($Na_2CO_3{\cdot}7H_2O$, PDF#76-1108), calcium sodium carbonate (shortite, $Ca_2Na_2(CO_3)_3$, PDF#72-1026) and calcium carbonate ($CaCO_3$, PDF#29-0305). Besides carbonates, a crystalline calcium aluminosilicate hydrated compound (garronite, $Na_2Ca_3Al_{12}Si_{20}O_{64}{\cdot}27H_2O$, PDF#85-1567) likely formed. The latter phase (a zeolite) is interesting, since it has been already reported to be formed by Na^+ incorporation in C-A-S-H gels, obtained by alkaline activation of slags and ashes [31–33]. Unlike soda-lime glass (leading to a tobermoritic gel, based on C-S-H), VBA glass was evidently prone to the formation of a truly geopolymeric-like (zeolitic) gel, amorphous (with no pre-curing) or semicrystalline (with pre-curing).

The new hardening mechanism was confirmed by the thermal analysis. The thermogravimetric analysis (TGA) of the initial VBA and hardened foam, after activation and the complete setting, is shown in Fig. 3a. The graph also reports the weight loss of the used surfactant (Triton X-100), normalised at 4 wt% (the amount of additive employed in the foaming process). Around 2 wt% of the weight loss below 200 °C on the hardened foam could be attributed to the release of physically bonded water, which is consistent with the wide endothermic bands in the DTA plot shown in Fig. 3b. This loss is much lower than the cases of glass suspensions hardened by C-S-H formation shown in previous studies [23–25]. The further weight loss, that is, of around 5.8 wt%, which occurred between 200 and 500 °C, could mostly be attributed to surfactant burn-out (≈4%, as shown in Fig. 2a), corresponding to the sharp exothermic peak at 300 °C in Fig. 3b. The remaining loss (1.8 wt%) should be attributed to the decomposition of newly developed phases; the thermal effects above 500 °C are hard to distinguish, as a result of the overlapping of oxidation reactions, which caused a slight weight increase in both the starting VBA and hardened VBA (see Fig. 2a).

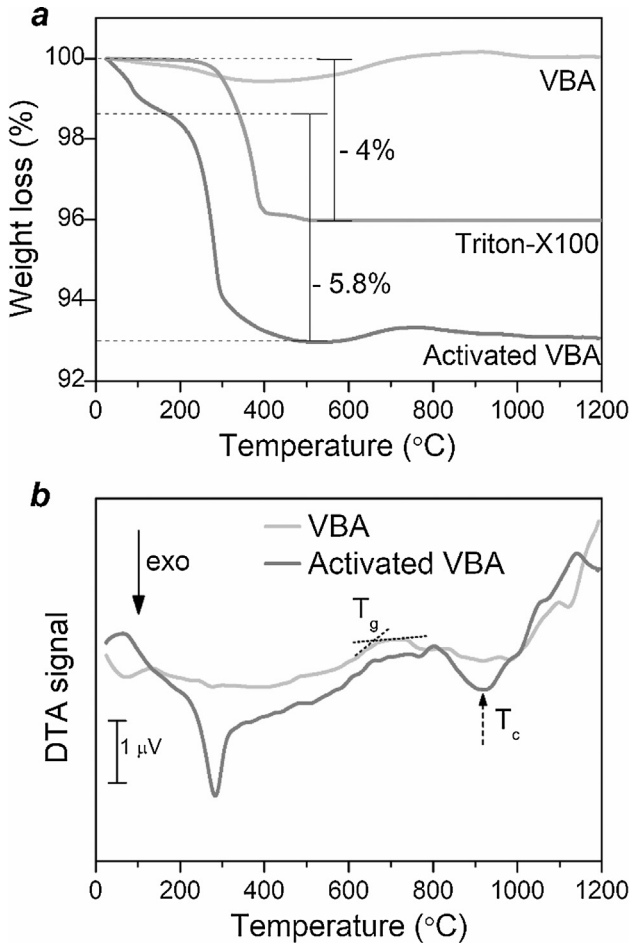

Fig. 3. Thermal analysis of the VBA glass before and after foaming; (a) Thermogravimetric plot of the VBA alkali-activated hardened foams and normalised Triton X-100; (b) Differential thermal analysis of the VBA glass powder and 'green' glass foam achieved as a result of alkali activation and direct foaming.

The glass transition of VGA was interpreted as occurring at 660 °C (T_g). Interestingly, a clear crystallization exothermic effect (peak centred at about 900 °C, see the arrow in Fig. 2b) was detected only in the activated VBA. In our opinion, this could be due to the formation of a low viscosity alkali-rich glass phase, between adjacent VBA glass granules, after the decomposition of the binding phases developed upon low temperature hardening. Alkali-enriched glasses are known to feature a lower apparent activation energy of crystal growth, so that they catalysed the crystallization [34]. A crystallization peak at 900–950 °C is consistent with the formation of calcium silicates (e.g. wollastonite, $CaSiO_3$) [35–37]; the reduction of the crystallization temperature, as an effect of the disruption the glass network (allowing rearrangement in turn favouring the cystallization) is also well known [38,39].

Fig. 4 shows the overall pore structure of the developed foams, by means of optical stereomicroscopy. The foams exhibited a high microstructural uniformity after activation and hardening, with a significant change due to the application of the pre-curing step; the foams that were not subjected to a pre-curing step presented pores with a diameter of 940 ± 40 μm, while the foams produced after 1 h of pre-curing consisted of much smaller cells, with a diameter of 330 ± 10 μm. The reduction in the pore size can be attributed to the increase in the viscosity of the glass suspension during the curing step, which prevented cell coalescence. The firing treatment had no substantial effect on the microstructure. The cells did not shown any sign of coarsening, and the openings between the adjacent cells were not sealed by a thin membrane, formed by viscous flow (as observed for soda-lime glass) [23]. The 'freezing' of the microstructure developed upon the low temperature foaming was attributed to the control of the viscous flow by the crystallization, as found for bioglass foams transformed into wollastonite and diopside glass-ceramic foams [24].

The differences in cell size, without or with the application of a pre-curing step, are again evident in Fig. 5a and b. The evolution of the samples after firing was further investigated by scanning electron microscopy for foams fired at 900 °C. As shown in Fig. 5c, the obtained foams actually exhibited a 'hierarchical' porosity, i.e. apart from the macro-pores that formed by gel-casting, some smaller pores appeared in the cell struts, which may have been due to gas release occurring during the decomposition of the hydrated compounds and carbonates. In addition, Fig. 5d testifies the occurrence of an intensive crystallization.

According to the mineralogical analysis shown in Fig. 6, sintering led to a substantial glass devitrification already at 800 °C, with formation of calcium silicates, as expected from thermal analysis. The developed phases consisted of wollastonite ($CaSiO_3$, PDF#76-0925) as well as of quite complex solid solutions of the pyroxene ($Mg_{0.89}Fe_{0.08}Al_{0.20}Cr_{0.04}Ti_{0.01}Ca_{0.76}Na_{0.10}Si_{1.92}O_6$, PDF#85-1827) and melilite ($(Ca_{1.96}Na_{0.05})(Mg_{0.24}Al_{0.64}Fe_{0.12})(Si_{1.39}Al_{0.61}O_7)$, PDF#72-2128) groups. Interestingly, when the firing temperature was increased to 900 °C, the melilite solid solution practically disappeared. This was concluded on the basis of the transformation of the melilite into additional wollastonite and pyroxene solid solution, which was consistent with the increase in the related peaks. The transformation of the melilite solid solution was likely due to an interaction with silica from the residual glass phase (if we refer, for the sake of simplicity, to the CaO-MgO-SiO_2 system, akermanite, $Ca_2MgSi_2O_7$ – a melilite solid solution end-member –,

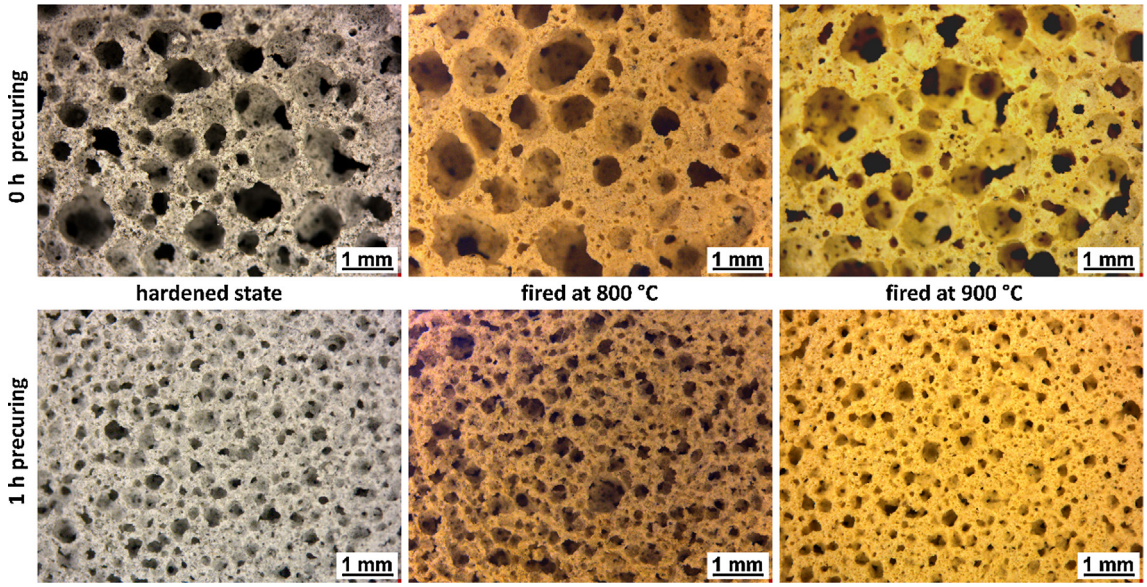

Fig. 4. Microstructural morphology of the VBA foams in the hardened state and after firing treatments (actual colours).

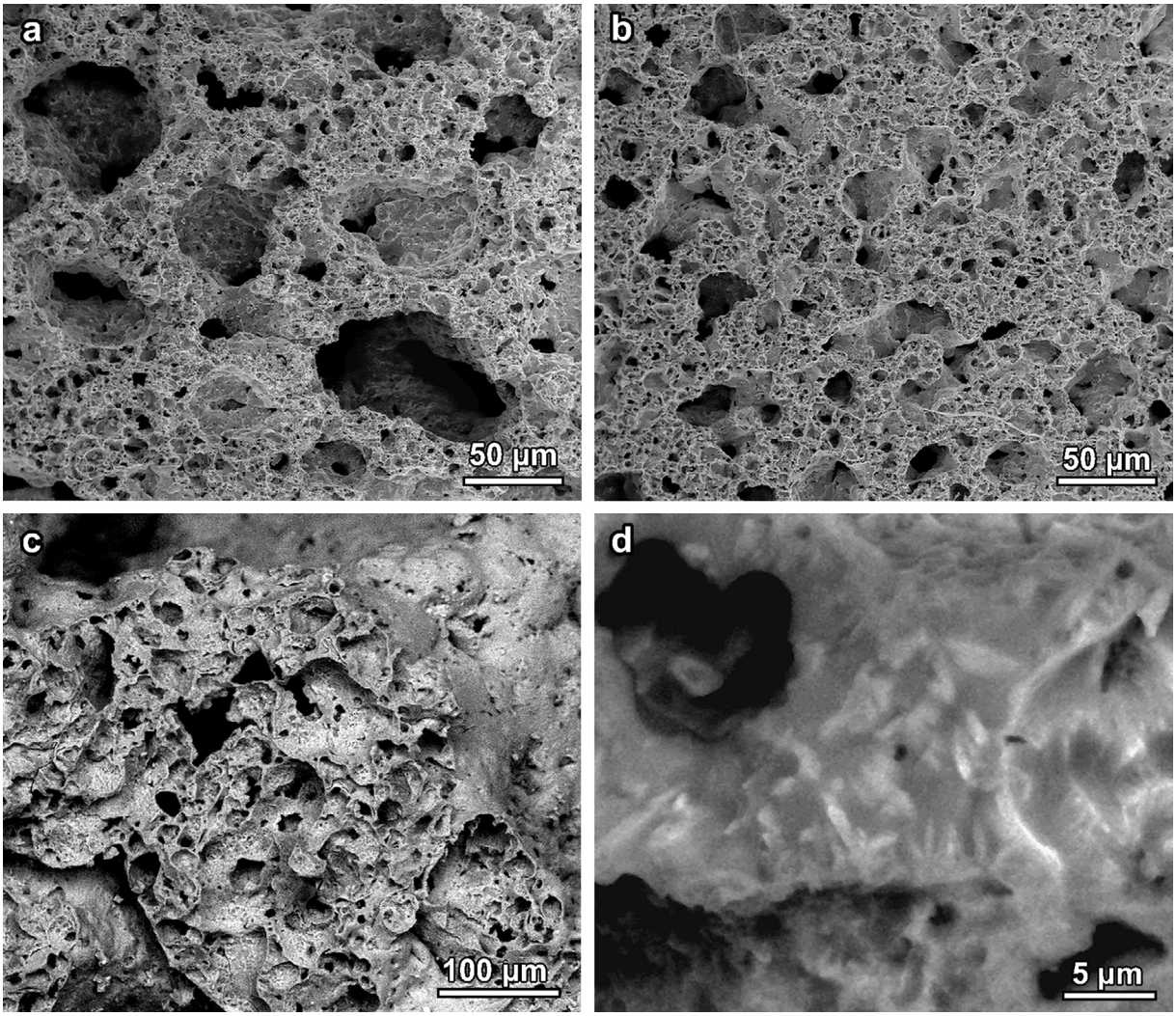

Fig. 5. High magnification morphology of the VBA foams in the hardened state and after a firing treatment at 900 °C: a) 0 h pre-curing; b) 1 h pre-curing; c and d) details of the strut structure (c) and solid phase (d) of a foam treated at 900 °C after 1 h of pre-curing.

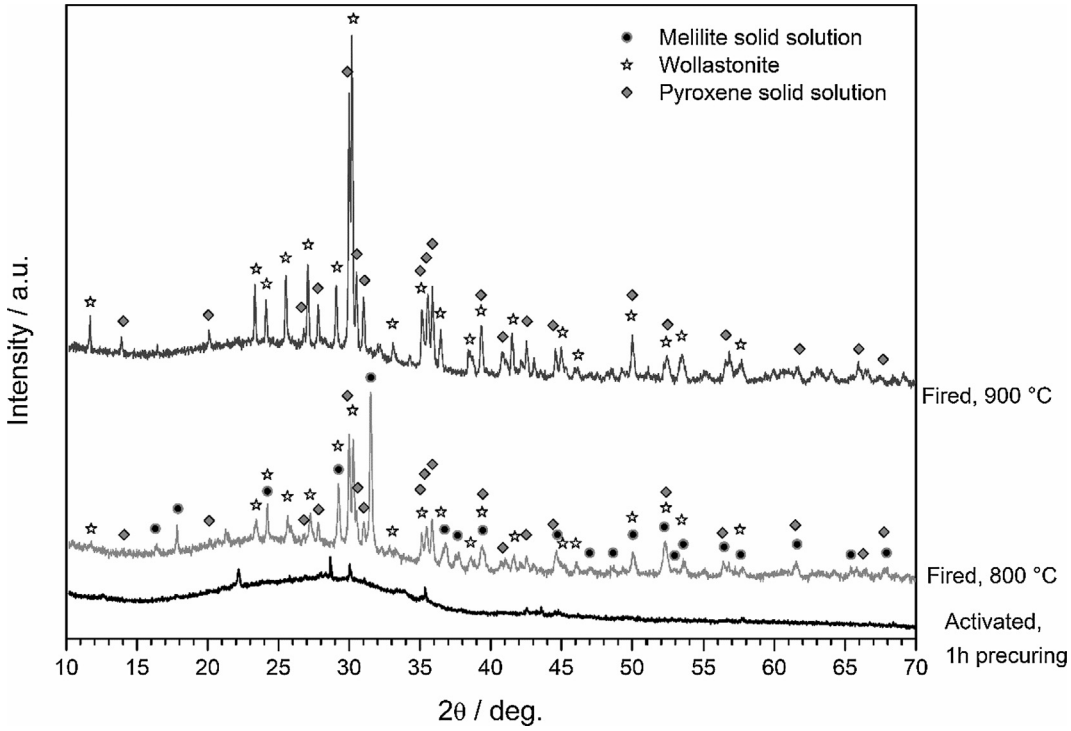

Fig. 6. X-ray diffraction patterns of VBA glass-based foams in the hardened state and after firing at 800 and 900 °C.

reacting with silica, may turn into a mixture of wollastonite and diopside, $CaMgSi_2O_6$ – a pyroxene end-member –, as follows: $Ca_2MgSi_2O_7 + SiO_2 \rightarrow CaSiO_3 + CaMgSi_2O_6$).

Table 2 shows that the increase in firing temperature, from 800 to 900 °C, only had a slight effect on the overall porosity and on the balance between the open and closed porosity thus further confirming the reduction in the viscous flow caused by crystallization. In particular, foams sintered at 900 °C reached an excellent crushing strength, if we consider the classical model proposed by Gibson and Ahsby [40]. According to this model, the crushing strength (σ_c) of a cellular body is conditioned by the bending strength of the solid phase (σ_{bend}) and by the porosity, expressed in terms of relative density (ρ_{rel}, defined as $\rho_{rel} = 1 - P/100$, where P is the total porosity). The corresponding overall equation is:

$$\sigma_c \approx \sigma_{bend}\left[C \cdot (\Phi \cdot \rho_{rel})^{3/2} + (1 - \Phi) \cdot \rho_{rel}\right] \quad (1)$$

C is a dimensionless calibration constant (~0.2). The quantity $(1 - \Phi)$ expresses the fraction of solid positioned at the cell faces. In the case of open-celled foams, with fully interconnected pores and solid material placed only on the cell edges, like in the present foams, we can think at $\Phi = 1$ $(1 - \Phi = 0)$.

$$\sigma_c \approx \sigma_{bend} \cdot C \cdot (\Phi \cdot \rho_{rel})^{3/2} \quad (2)$$

Eq. (2) may be used to assess, from experimental values of σ_c and ρ_{rel}, the strength of the solid phase. As reported in the same table (square brackets), the calculated bending strength of the solid phase of the foams processed with no pre-curing and fired at 900 °C exceeded 190 MPa, a level that is in good agreement with the bending strength of monolithic glass-ceramics [13]. The increase in the crushing strength (corresponding to a calculated bending strength above 320 MPa), for the foams fired at 900 °C, but processed with 1 h pre-curing, is consistent with the observed decrease in the cell size (see Fig. 3). The cell size is not comprised in the Gibson and Ashby model (Eqs. (1) and (2)), but it is well known that, at a given relative density, the strength of ceramic foams increases dramatically with decreasing cell size [41]. The particurly high strength, combined with open porosity, makes the developed materials quite promising for many structural applications (e.g. as thermal insulators in buildings or as filters).

Waste-derived materials, before any application, should be subjected to a careful analysis of the chemical stability. In the present investigation, the foams fired at 900 °C were compared with the as received VBA, according to the EN 12457-2 leaching test. Table 3 shows that the VBA was particularly stable, with all the analysed metal ions below the detection limit of the ICP device. The leaching of the VBA, after transformation into glass-ceramic foams, was essentially above the detection limits, but this was not surprising.

Table 2
Physical and mechanical properties of the heat treated glass ceramic foams.

Pre-curing	Firing T (°C)	Density, ρ (g/cm³)			Porosity (%)			Crushing strength, σ_c (MPa) [σ_{bend} (MPa)]
		Geometric	Apparent	True	Total	Open	Closed	
0 h	800	0.43 ± 0.01	2.11 ± 0.01	2.64 ± 0.01	83 ± 2	79 ± 2	4 ± 1	2.2 ± 0.1
	900	0.45 ± 0.01	2.43 ± 0.05	2.79 ± 0.01	83 ± 2	81 ± 4	2 ± 2	2.7 ± 0.2 [192.6]
1 h	800	0.48 ± 0.01	2.55 ± 0.05	2.66 ± 0.01	82 ± 2	81 ± 4	0 ± 2	1.5 ± 0.1
	900	0.59 ± 0.02	2.72 ± 0.02	2.85 ± 0.01	79 ± 2	77 ± 3	2 ± 1	6.2 ± 0.7 [322.1]

Table 3
Results of the leaching tests on the selected glass ceramic foams.

Element (ppm)	VBA as received (ppm)	900 °C (ppm)		Limits [2003/33/EC, 2003] (ppm)	
		0 h gel	1 h gel	Inert material	Non-hazardous material
As	<0.0049	<0.0049	<0.0049	0.5	2
Ba	<0.0000	<0.0000	<0.0000	20	100
Cd	<0.0002	0.0006	0.0004	0.04	1
Cr	<0.0004	0.0011	0.0008	0.5	10
Cu	<0.0001	0.0125	0.0003	2	50
Mo	<0.0033	<0.0033	<0.0033	0.5	10
Ni	<0.0014	<0.0014	<0.0014	0.4	10
Pb	<0.0047	0.0125	0.0157	0.5	10
Se	<0.0122	0.0617	0.0526	0.1	0.5
Zn	<0.0203	0.0146	<0.0203	4	50

In fact, due to the complex redistribution of ions in the crystal phases and in the residual glass phase (with a new chemical composition) [26], each possesses a different chemical resistance. However, the leachates of the glass-ceramics remained well below the limits for inert materials; the foams may be reputed as being safe, considering that they were tested in the form of porous fragments that feature a much-enhanced specific surface, compared to the solid fragments of the as received VBA (in other words, the leaching test on foams was much more severe).

4. Conclusions

We may conclude that:

- The approach to glass-ceramic foams by means weak alkali activation of glass suspensions/mechanical foaming/sintering can be extended to vitrified bottom ash (VBA);
- Unlike previously studied glasses, in the present experiment, suspensions of powdered vitrified bottom ash underwent hardening, mainly through the formation of carbonate phases, which later decomposed upon firing;
- Sintering at 800–900 °C did not lead to any substantial 'reshaping' of the pores that formed upon low temperature mechanical foaming, due to the significant crystallisation that was stimulated by the same alkali activation;
- The pore size can be adjusted by operating on the low temperature mechanical foaming step, by applying a 'pre-curing' step; with the adopted solid/liquid ratio, the porosity remained practically constant about 80% (mostly open);
- The crystallization of VBA led to porous glass-ceramics that had excellent crushing strength, for the given, substantial porosity, with no significant degradation of chemical stability, compared to the parent glass.

5. Summary of novel conclusions

- Highly porous glass-ceramics from vitrified MSWI bottom ash were obtained by 'inorganic gel casting' (mechanical foaming of suspensions undergoing progressive hardening)
- The hardening occurred with a low molarity alkaline solution, through the formation of carbonate phases
- Hardened foams were transformed into glass-ceramic foams through a sinter-crystallisation process by firing at 800–900 °C.
- The chemical stability and the leaching of heavy metals of the final product remained under the thresholds specifications

Conflict of interest

None.

Acknowledgements

The research leading to these results has received funding from the European Union's Horizon 2020 research and innovation programme under the Marie Sklodowska-Curie grant agreement No. 642557 (CoACH—ETN: Advanced glasses, Composites And Ceramics for High growth Industries European Training Network).

References

[1] Eurostat, 2016, 'Waste database municipal waste' <http://appsso.eurostat.ec.europa.eu/nui/show.do?dataset=env_wasmun&lang=en>, (accessed 13.04.18).
[2] Best Available Techniques (BAT) Reference Document on Waste Incineration Industrial Emissions Directive 2010/75/EU (Integrated Pollution Prevention and Control) JOINT RESEARCH CENTRE Institute for Prospective Technological Studies Directorate B – Growth and Innovation Sustainable Production and Consumption Unit Circular Economy and Industrial Leadership Unit European IPPC Bureau DRAFT 1 (May 2017).
[3] P.H. Brunner, H. Rechberger, Waste to energy – key element for sustainable waste management, Waste Manage. 37 (2015) 3–12.
[4] M. Margallo, M.B.M. Taddei, A. Hernández-Pellón, R. Aldaco, A. Irabien, Environmental sustainability assessment of the management of municipal solid waste incineration residues: a review of the current situation, Clean Technol. Environ. Policy 17 (2015) 1333–1353.
[5] S. Toller, E. Kärrman, J.P. Gustafsson, Y. Magnusson, Environmental assessment of incinerator residue utilisation, Waste Manage. 29 (2009) 2071–2077.
[6] O. Hjelmar, J. Holm, K. Crillesen, Utilisation of MSWI bottom ash as sub-base in road construction: First results from a large-scale test site, J. Hazard. Mater. 139 (2007) 471–480.
[7] E. Toraldo, S. Saponaro, A road pavement full-scale test track containing stabilized bottom ashes, Environ. Technol. 36 (2015) 1114–1122.
[8] R. del Valle-Zermeño, J. Formosa, J.M. Chimenos, M. Martínez, A.I. Fernández, Aggregate material formulated with MSWI bottom ash and APC fly ash for use as secondary building material, Waste Manage. 33 (2013) 621–627.
[9] X. Li, Y. Lv, B. Ma, Q. Chen, X. Yin, S. Jian, Utilization of municipal solid waste incineration bottom ash in blended cement, J. Cleaner Prod. 32 (2012) 96–100.
[10] B. Zhang, C.S. Poon, Use of Furnace Bottom Ash for producing lightweight aggregate concrete with thermal insulation properties, J. Cleaner Prod. 99 (2015) 94–100.
[11] U. Müller, K. Rübner, The microstructure of concrete made with municipal waste incinerator bottom ash as an aggregate component, Cem. Concr. Res. 36 (2006) 1434–1443.
[12] P.A. Bingham, R.J. Hand, Vitrification of toxic wastes: a brief review, Adv. Appl. Ceram. 105 (2006) 21–31.
[13] A. Rincón, M. Marangoni, S. Cetin, E. Bernardo, Recycling of inorganic waste in monolithic and cellular glass-based materials for structural and functional applications, J. Chem. Technol. Biotechnol. 91 (2016) 1946–1961.
[14] M. Ferraris, M. Salvo, A. Ventrella, L. Buzzi, M.M. Veglia, Use of vitrified MSWI bottom ashes for concrete production, Waste Manage. 29 (2009) 1041–1047.
[15] A. Saccani, F. Sandrolini, F. Andreola, L. Barbieri, A. Corradi, I. Lancellotti, Influence of the pozzolanic fraction obtained from vitrified bottom-ashes from MSWI on the properties of cementitious composites, Mater. Struct. 38 (2005) 367–371.
[16] S. Yang, W. Chiu, T. Wang, C. Chen, C. Tzeng, Porous materials produced from incineration ash using thermal plasma technology, Waste Manage. 34 (2014) 1079–1084.
[17] G. Scarinci, G. Brusatin, L. Barbieri, A. Corradi, I. Lancellotti, P. Colombo, S. Hreglich, R. Dall'Igna, Vitrification of industrial and natural wastes with production of glass fibres, J. Eur. Ceram. Soc. 20 (2000) 2485–2490.
[18] L.M. Schabbach, G. Bolelli, F. Andreola, I. Lancellotti, L. Barbieri, Valorization of MSWI bottom ash through ceramic glazing process: a new technology, J. Cleaner Prod. 23 (2012) 147–157.

[19] R.D. Rawlings, J.P. Wu, A.R. Boccaccini, Glass-ceramics: Their production from wastes—a review, J. Mater. Sci. 41 (2006) 733–761.
[20] P. Appendino, M. Ferraris, I. Matekovits, M. Salvo, Production of glass–ceramic bodies from the bottom ashes of municipal solid waste incinerators, J. Eur. Ceram. Soc. 24 (2004) 803–810.
[21] M. Ferraris, M. Salvo, F. Smeacetto, L. Augier, L. Barbieri, A. Corradi, I. Lancellotti, Glass matrix composites from solid waste materials, J. Eur. Ceram. Soc. 21 (2001) 453–460.
[22] S. Qian, J. Lin, B. Tang, Preparation of glass foams from vitrified municipal solid waste incinerator ash, J. Chin. Ceram. Soc. 42 (2014) 108–112.
[23] A. Rincón, G. Giacomello, M. Pasetto, E. Bernardo, Novel 'inorganic gel casting' process for the manufacturing of glass foams, J. Eur. Ceram. Soc. 37 (2017) 2227–2234.
[24] H. Elsayed, A. Rincon, L. Ferroni, C. Gardin, B. Zavan, E. Bernardo, Bioactive glass-ceramic scaffolds from novel 'inorganic gel casting' and sinter-crystallization, Materials 10 (2017) 171.
[25] A. Rincón, D. Desideri, E. Bernardo, Functional glass-ceramic foams from 'inorganic gel casting' and sintering of glass/slag mixtures, J. Cleaner Prod. 187 (2018) 250–256.
[26] P. Rabelo Monich, A. Rincón, D. Höllen, E. Bernardo, Porous glass-ceramics from alkali activation and sinter-crystallization of mixtures of waste glass and residues from plasma processing of municipal solid waste, J. Cleaner Prod. 188 (2018) 871–878.
[27] I. Lancellotti, C. Ponzoni, L. Barbieri, C. Leonelli, Alkali activation processes for incinerator residues management, Waste Manage. 33 (2013) 1740–1749.
[28] I. Lancellotti, M. Catauro, C. Ponzoni, F. Bollino, C. Leonelli, Inorganic polymers from alkali activation of metakaolin: Effect of setting and curing on structure, J. Sol. State Chem. 200 (2013) 341–348.
[29] Z. Chen, Y. Liu, W. Zhu, E. Yang, Incinerator bottom ash (IBA) aerated geopolymer, Constr. Build. Mater. 112 (2016) 1025–1031.
[30] F. Allali, E. Joussein, N. Idrissi Kandri, S. Rossignol, The influence of calcium content on the mixture of sodium silicate with different additives: Na2CO3, NaOH and AlO(OH), Constr. Build. Mater. 121 (2016) 588–598.
[31] J.L. Provis, S.A. Bernal, Geopolymers and related alkali-activated materials, Annu. Rev. Mater. Res. 44 (2014) 299–327.
[32] S.K. Nath, S. Kumar, Reaction kinetics, microstructure and strength behavior of alkali activated silico-manganese (SiMn) slag – fly ash blends, Constr. Build. Mater. 147 (2017) 371–379.
[33] S.K. Nath, S. Kumar, Influence of granulated silico-manganese slag on compressive strength and microstructure of ambient cured alkali-activated fly ash binder, Waste Biomass Valorization (2018), https://doi.org/10.1007/s12649-018-0213-1.
[34] T. Watanabe, H. Hashimoto, M. Hayashi, K. Nagata, Effect of alkali oxides on crystallization in $CaO–SiO_2–CaF_2$ glasses, ISIJ Int. 48 (2008) 925–933.
[35] R.P. Sreekanth Chakradhar, B.M. Nagabhushana, G.T. Chandrappa, K.P. Ramesh, J.L. Rao, Solution combustion derived nanocrystalline macroporous wollastonite ceramics, Mat, Chem. Phys. 95 (2006) 169–175.
[36] H. Arstila, E. Vedel, L. Hupa, M. Hupa, Factors affecting crystallization of bioactive glasses, J. Eur. Ceram. Soc. 27 (2007) 1543–1546.
[37] A. Karamanov, M. Pelino, Induced crystallization porosity and properties of sintereds diopside and wollastonite glass-ceramics, J. Eur. Ceram. Soc. 28 (2008) 555–562.
[38] R.G. Hill, C. Goat, D. Wood, Thermal analysis of a SiO_2-Al_2O_3-CaO-CaF_2 glass, J. Am. Ceram. Soc. 75 (1992) 778–785.
[39] A. Calver, R.G. Hill, A. Stamboulis, Influence of fluorine content on the crystallization behavior of apatite-wollastonite glass-ceramics, J. Mater. Sci. 39 (2004) 2601–2603.
[40] L.J. Gibson, M.F. Ashby, Cellular Solids: Structure and Properties, Cambridge University Press, Cambridge, UK, 1999.
[41] R. Brezny, D.J. Green, The effect of cell size on the mechanical behavior of cellular materials, Acta Metall. Mater. 38 (1990) 2517–2526.